Front End Simulation for a double Phase Rotation Neutrino Factory

ICOOL Simulation of PJK

R.B. Palmer, S. Berg, R. Fernow, J. Gallardo, H. Kirk, R. Weggel

Brookhaven National Laboratory

Y. Fukui

UCLA

C. Kim, E. Kim, G. Penn, J. Wurtele

UCB

N. Mokhov

FNAL

April 11, 2000

Abstract

Results are presented of a complete MARS/ICOOL simulation of a double phase rotation neutrino factory front end similar to that described in the paper of Palmer, Johnson and Keil (PJK). Differences include the use of a smaller radius mercury target, the first rf cavity has been moved to 6.3 m from the target, added field reversals in the mini cooling and long drift, and the use of FOFO cooling. The first phase rotation uses 6 MV/m rf at 30 MHz, the second uses a ± 0.55 MV/m induction linac. The FOFO cooling lattice is similar to that proposed at LBL, but has lower current densities. After cooling, the simulation gives a total of 0.18 muons per proton, with 0.15 muons per proton within a longitudinal acceptance cut of 71 π

mm, and a transverse acceptances of 9.35 π mm rad. A comparison is made with the performance of similar systems with different targets, proton energy, number of phase rotations and length.

Contents

List of Figures

List of Tables

1. Introduction

The work reported here has been done within the Muon Collider Collaboration, and owes much to its many members. The scenario given is based on the work of Palmer, Johnson and Keil (PJK)[1] as discussed in the scenarios working group at Lyon[2]. The simulations used in that work (for pion production[3], MCM[4] for phase rotation, a mere estimate for bunching and an earlier version of ICOOL[5] for the cooling) contained many approximations. The current work uses MARS[6] for pion production, and *ICOOL*[5] for all the rest. The system described was optimized, and the numbers and plots shown were obtained using ICOOL version 1.99. The data files run on ICOOL version 2.03, but give slightly different values.

- The postscript file of this paper is at

  `http://pubweb.bnl.gov/people/palmer/nu/pjksim/pjksim.ps`

- The TEX files of this paper can be found at

  `http://pubweb.bnl.gov/people/palmer/nu/pjksim/tex/`

- The icool files used (it is a single run) are at

  `http://pubweb.bnl.gov/people/palmer/nu/pjksim/icool/`

The components of the Front End are:

- A target and pion capture system consisting of a mercury target in a 20 T solenoid, with a field tapering down to 1.25 T.
- Phase rotation, in 2 stages, to reduce the muon energy spread at the expense of spreading them out over a longer time interval. The system is designed to correlate the muon polarization with time, allowing control of the relative intensity of muon and anti-electron neutrinos.

- A limited amount of cooling.

- This Front End would be followed by a fast muon acceleration to 20 GeV or more, in a system of linac and one or two recirculating linear accelerators (RLAs). The beam would then be injected into a storage ring with long straight sections pointing to a distant neutrino detectors for oscillation studies, and to one or more near detectors for high intensity studies.

A. Definitions and conventions

Emittances, whether stated or not, are always taken to be normalize rms values:

$$\epsilon_n = \beta_v \gamma_v \sqrt{< x^2 >< x'^2 > - < x >^2 < x' >^2 - < xx' >^2} \tag{1}$$

For transverse emittances x is the transverse dimension x, or y; x' is the angle with respect to the axis in the same direction: x, or y (θ_x or θ_y) . In the longitudinal direction, x is the axial distance of the particles from the bunch center, and x' is the dimensionless momentum difference from the average momentum, divided by the average ($\frac{d\bar{p}}{p}$).

Thus, ignoring correlations:

$$\epsilon_n = \beta_v \gamma_v \sigma_x \sigma_{x'} \tag{2}$$

Acceptances are defined in terms of amplitude parameters J, the definition of which, ignoring correlations, are:

$$J_\perp = \beta_v \gamma_v \, \frac{\frac{x^2}{\beta} + x'^2 \beta + \frac{y^2}{\beta} + y'^2 \beta}{4} \tag{3}$$

$$J_{||} = \beta_v \gamma_v \frac{\frac{z^2}{\beta_s} + (\frac{dp}{p})^2 \beta_s}{2} \tag{4}$$

β_s is the synchrotron $\beta_s = \sigma_z/(\sigma_p/p)$. The lack of correlations means that α's are zero in all dimensions. With this convention, the average of the J's are equal to the normalized emittances, as defined above. The average of any one term would gives the emittance, hence the number in the denominator equals the number of terms. Note that the x and y amplitudes are combined to correspond to circular apertures, but the definitions are for the normally defined separate x and y emittances.

2. Components

A. Proton Source

The following table gives the assumed parameters of the 24 GeV proton driver. It includes those for a potential upgrade to 4 MW, and those for 16 GeV drivers at 1 and 4 MW.

TABLES

Table 1. Parameters of proton drivers at BNL and Fermilab.

		AGS-BNL	AGS-BNL	FermiLab	FermiLab
Energy	GEV	24	24	16	16
Power	MW	1	4	1	4
Repetition	Hz	2.5	5	15	15
p's/fill		10^{14}	$2\ 10^{14}$	$2.5\ 10^{13}$	10^{14}
bunches		6	6	4	4
circumference.	m	807	807	474	474
spacing	m	135	135	118	118
σ_t	ns	1	1	1	1

B. Target and Capture

It is assumed here that the liquid mercury jet solution is used. Pion production from the target, assumed in a 20 T uniform solenoidal field, was calculated by MARS and written to a file at the target end. The events in this file, from 100,000 protons, have weights varying over several orders of magnitude and can cause larger statistical errors than given by normal statistics. Thus this file is used to generate a shorter file containing 5000 uniformly weighted events, and this file is used as input to ICOOL[5] for the rest of the simulation.

The dimensions and angle of the target were obtained from an optimization performed by H. Kirk[7]:

Table 2. Parameters of the liquid mercury jet

material	Hg
radius (mm)	3
length (m)	0.3
angle (rad)	0.15
solenoid field (T)	20
solenoid radius (cm)	7.5

The calculated temperature rise in such a target, for the AGS 1 MW case, assuming constant specific heat, is 5000 degrees. It is clear that the assumption of constant specific heat is wrong, but the number serves to indicate a likely rapid evaporation of the jet. If such evaporation occurs before the end of the spill (2 microseconds for the AGS case) then the target efficiency for the later bunches may be very low. Possible solutions to this problem are discussed in the last section. The situation is not so serious in the Fermilab case.

The capture solenoid is also assumed to be the same as in the muon collider status report[8], and is assumed to be an uniform $B_z = 20$ T. This is followed by a field taper down to 1.25 T, as given by Y. Fukui[9]. The Tb.3 gives the position, length, and radii of the current sheets used. The current densities j given assume coil thicknesses of 20 cm and are not intended to be realistic.

Table 3. Parameters of the current sheets used in the simulation.

z m	Len m	rad m	j $Amps/mm^2$
-2.5	1.2	.45	50
-1.3	1.6	.45	26.5625
-1.3	2.08	.17	17.30769
.3	.24	.45	177.0833
.54	.24	.45	148.125
.78	.24	.45	235.4167
1.02	.24	.65	227.0833
1.26	.24	.65	173.75
1.5	.24	.85	163.5417
1.74	.24	.85	132.0833
1.98	.24	1.05	103.3333
2.22	.48	1.05	40.3125

2.7	.7	1.25	25
3.4	.6	1.5	20
4	1	1.5	6.5
5	1	1.5	5.355
6	2	1.5	2.6775
8	2	1.5	2.6775
10	2	1.5	2.6775

The following plots show the positions of these sheets, the fields they generate (blue) and an ideal field profile (red) following the form: $B = \frac{B_o}{1+kL}$ where B_o is 20 T and $k = 1.8$.

FIGURES

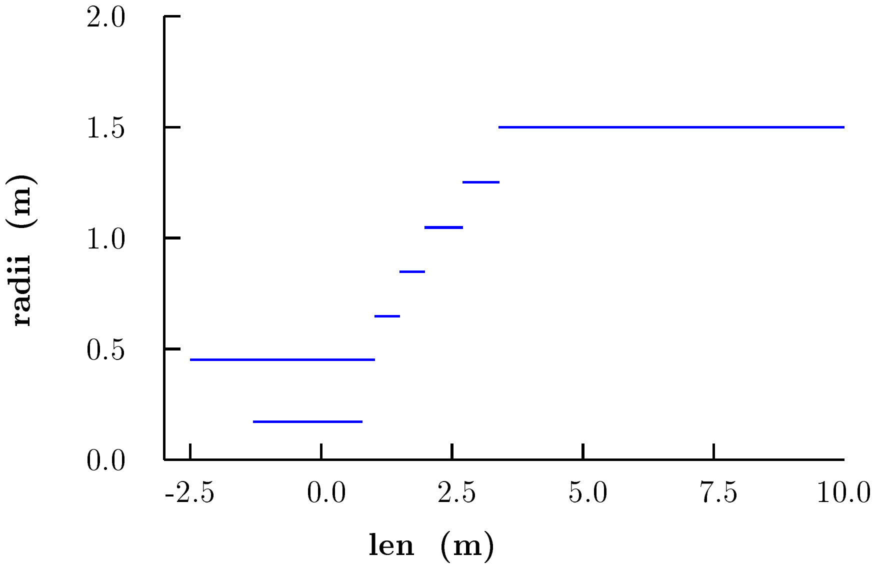

Fig. 1.

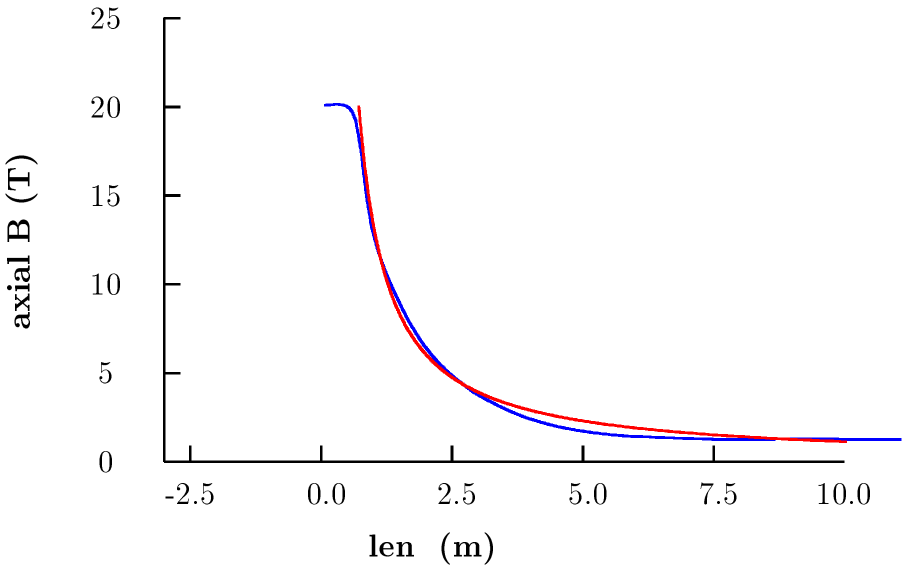

Fig. 2.

C. Phase Rotation #1

An early, high gradient, phase rotation is required if polarization is to be selected without particle loss. Forward decays, having one polarization, yield higher energy muons than backward decays which have the other polarization.

At the end of this first stage, the bunch length has increased by a factor of 6 and the energy spread has decreased by the same amount. The following Tb.4 gives parameters obtained with an initial proton energy of 24 GeV. One can assume that for an initial energy of 16 GeV, the ratio of muons to protons would be 2/3 of the values shown. The performance numbers are given for the particles between a *ct* of -2.5 and + 6 m, as shown in the Fig.3. It should be noted that this cut is not physical, is used only for the parameters in the tables and plots of the first phase rotation, and do not apply to the final muon plots.

At the end of this first rotation, the simulated energy *vs.* time distribution is shown in Fig.3.

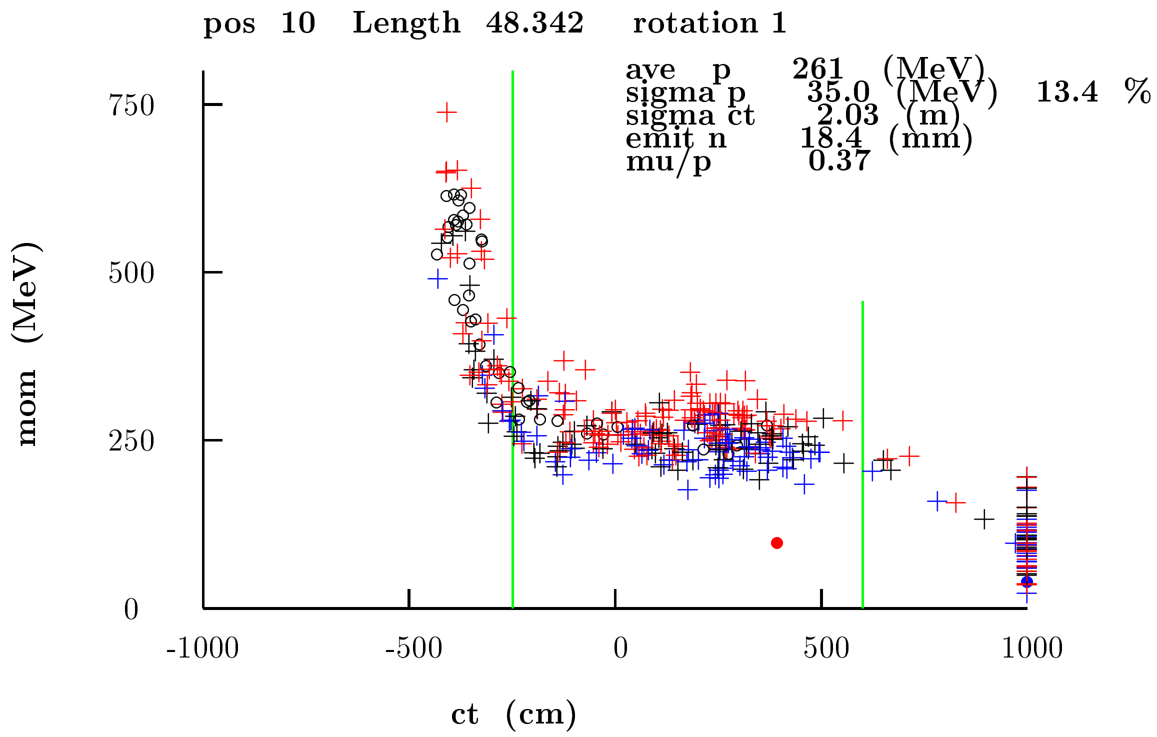

Fig. 3. Longitudinal phase space at the end of phase rotation No. 1

Table 4. Parameters of the first phase rotation.

	len	rad	B	f	grad	n_μ/n_p	σ_{ct}	$< E >$	dE/E	emit
	m		T	MHz	MV/m		m	MeV	%	π mm
target	.3	.03	20			1.02				
match	6.3	.6	1.25			0.6				
rf	12	.6	1.25	40	5					
rf	37	.6	1.25	30	5					
rf	5	.6	1.25	45	6	.37	2.0	260	13	18

In this and following plots the color and symbols indicate polarization and particle type:

$$\begin{array}{cc} \textit{red} & P > .3 \\ \textit{black} & .3 > P > -.3 \\ \textit{blue} & -.3 < P \\ + & \mu \\ o & \pi \\ \bullet & e \end{array} \tag{5}$$

D. Mini Cooling

Mini-cooling reduces the muon energies so that the subsequent drift length for a second phase rotation could be kept short. It also lowers the transverse emittance.

The mini cooling was done in two hydrogen absorbers in a fixed magnetic fields of 1.25 T; between the two, there is a matched field reversal in order to remove canonical angular momentum generated by the energy loss in the absorbers.

Table 5. Parameters of the mini-cooling cells

	len	rad	B	f	grad	n_μ/n_p	σ_{ct}	$< E >$	dE/E	emit
	m		T	MHz	MV/m		m	MeV	%	π mm
mini-cooling 1	3.2	.3	1.25			.36	2.0	200	100	20
B reversal	16.1	.6								
mini-cooling 2	.7	.3	1.25			.36	2.3	175	111	25

The following figure shows the energy vs time after the mini cooling.

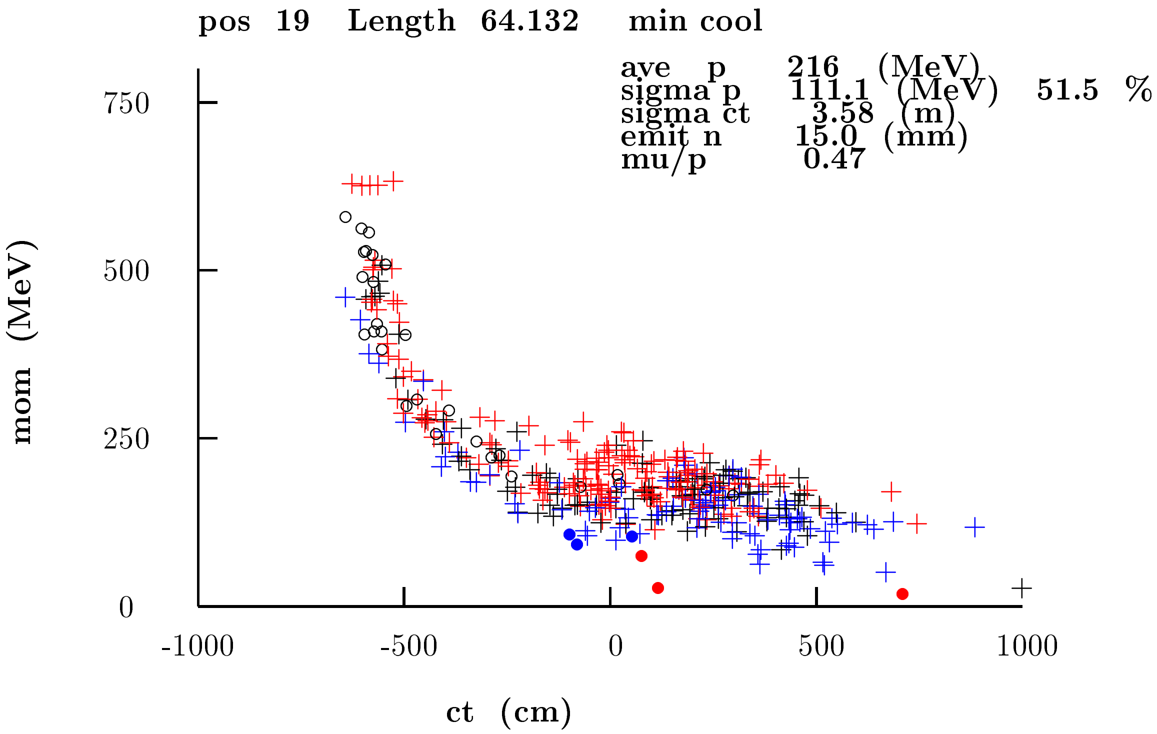

Fig. 4. Longitudinal phase space at the end of mini-cooling section

E. Phase Rotation #2

The object of this component is to further reduce the momentum spread at the expense of lengthening the bunch up to a distance of 90 m, approaching the initial proton bunch spacing ($\approx 135\ m$). The very long resulting bunch is then re-bunched at a higher frequency (175 MHz), yielding a train of about 50 individual muon bunches for every initial proton one. In addition, this second rotation results in the polarization being correlated with time, *i.e.* bunch number, instead of energy. The polarization is now preserved.

The rotation is performed by two drifts (80 m & 50 m) with a field reversal between them (20 m), followed by energy correction using an induction linac.

The coils used to reverse the fields are shown in Fig.5 and Tb.6. Their current densities are low, but their radii are unnecessarily large for historical reasons. There should be even less problem in obtaining the desired field profile with smaller radius coils.

Table 6. Parameters of the coil set used to control the growth of canonical momentum

len1	dl	rad	dr	sheets	I/A
m	m	m	m		A/mm^2
0.000	6.500	1.000	0.050	3	20.07
6.973	0.650	1.000	0.050	2	34.71
8.999	0.700	1.000	0.050	2	56.38
10.301	0.700	1.000	0.050	2	-56.38
12.377	0.650	1.000	0.050	2	-34.71
dvi 13.500	6.500	1.000	0.050	3	-20.07

The axial B fields and betas in the field reversal are shown below in Fig.6:

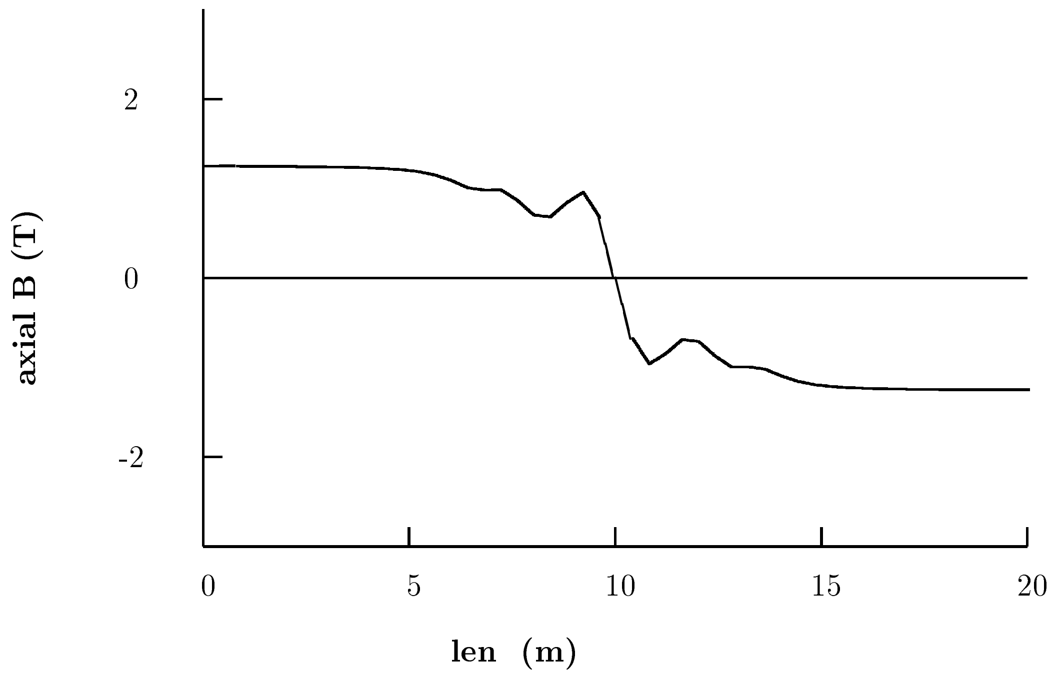

Fig. 5. Set of coils used to reverse the field in order to control the growth of canonical angular momentum

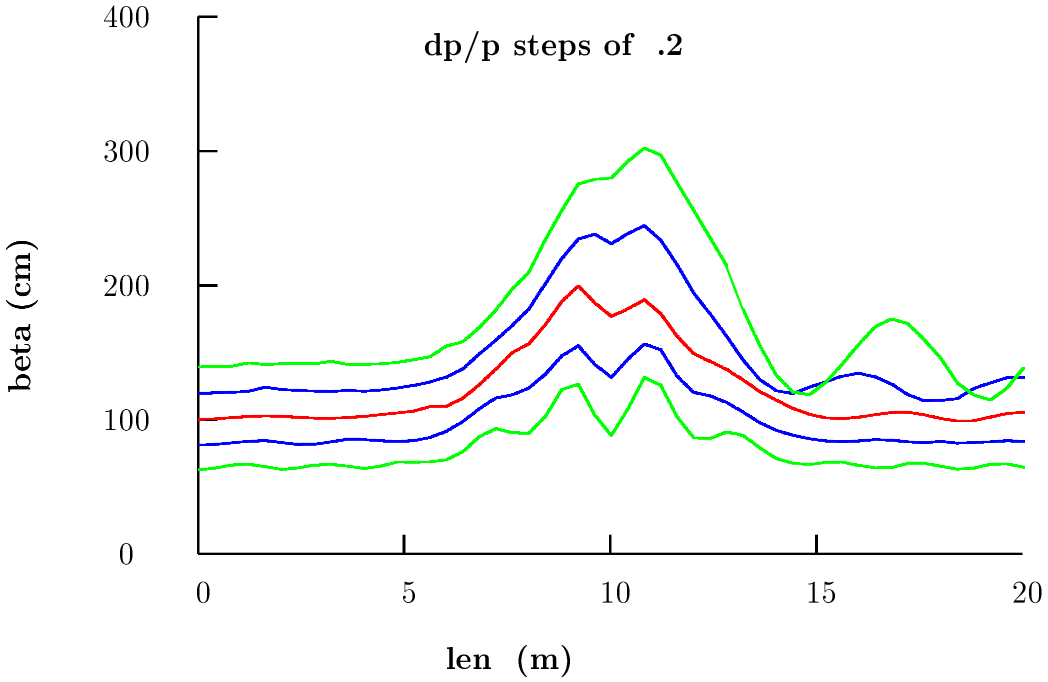

Fig. 6. B field and β

The Induction linac ($\pm$80 MeV acceleration) has a single pulse shape tailored to correct the time-energy correlation generated by the drift. It is simulated here by a sequence of sinusoidal rf fields. The induction linac must supply a rapid train of accelerations, spaced by the proton bunch spacing (135 m), and equal in number to the number of proton bunches. The wave form used is thus made up of harmonics (2.2, 4.4, and 8.8 MHz) of the bunch spacing (2.2 MHz).

The following figures show the energy *vs.* the length of the muon bunch (c-time) before correction, the energy change from the induction linac, the energy *vs.* c-time the energy correction, and the polarization *vs.* c-time.

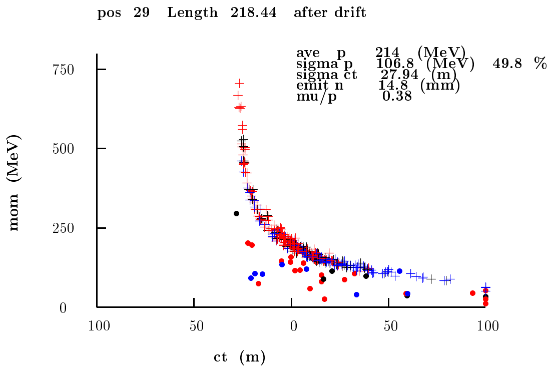

Fig. 7. Longitudinal phase-space at the end of the long drift

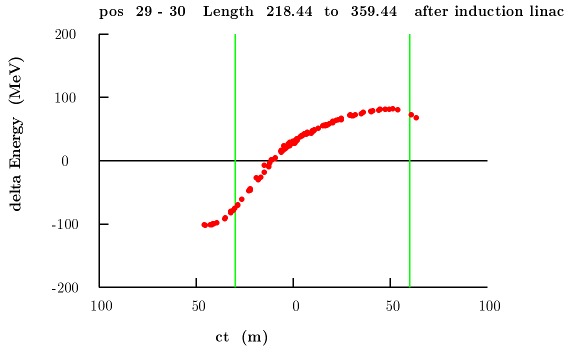

Fig. 8. Energy change *vs.* the length of the muon bunch (c-time)

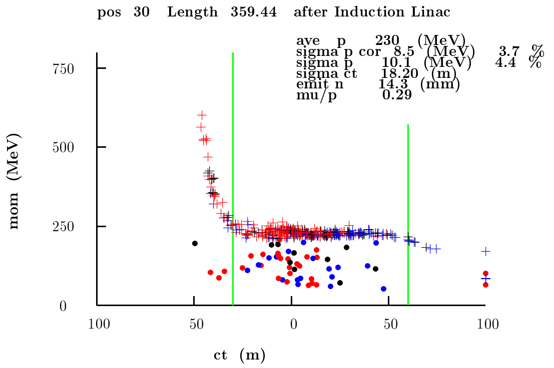

Fig. 9. Longitudinal phase-space at the end of phase rotation No. 2

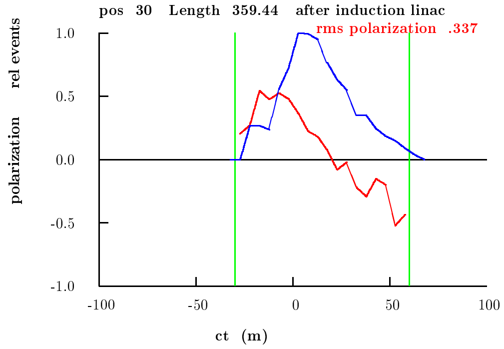

Fig. 10. Polarization *vs.* c-time (m)

The sensitivity of the maximum polarization to the initial proton bunch length is:

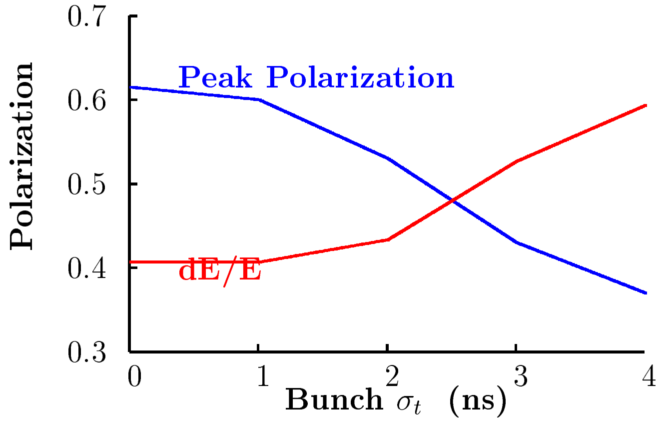

Fig. 11. Polarization *vs.* the proton bunch length.

- *rms* Polarization = 0.35
- dp/p intrinsic (i.e. with amp-mom correlation removed) 3.7 %

Table 7. Parameters of the phase rotation No. 2

	len	rad	B	freq.	grad	n_μ/n_p	σ_{ct}	$< E >$	dp/p	emit
	m		T	MHz	MV/m		m	MeV	%	π mm
drift 1	80	.3	1.25			.38				
B reversal	20	.6				.38				
drift 1	50	.3	1.25			.38				
Ind Lin	141	.3	1.25	2.2-8.8	+/- .55	.29	18	230	3.7	14

In this simulation, the B field in the induction linac is taken as fixed at 1.25 T. However, higher fields may be prefered for induction linac cost and amplitude-energy correlation matching reasons.

F. Matching into FOFO lattice

A sequence of solenoids is introduced to match the beta's from the fixed solenoid, of the phase rotation and induction linac, to a FOFO lattice. The coil details used (given in Tb.8 and Fig.12) are not realistic, their current densities are too high, but the B fields are reasonable and a suitable coil system will be designed after the focusing in the induction linac is established.

Table 8.

len1	dl	rad	dr	sheets	I/A
m	m	m	m		A/mm^2
0000	7.7	0.730	0.250	3	-4.07
7.700	0.650	0.730	0.250	3	-4.07
8.700	0.250	0.730	0.150	3	-16.42
9.250	0.250	0.730	0.150	3	-109.74
9.650	0.250	0.730	0.150	3	108.11
10.200	0.250	0.730	0.150	3	112.00
10.750	0.250	0.730	0.150	3	-112.00
11.300	0.250	0.730	0.150	3	-116.00
11.850	0.250	0.730	0.150	3	124.00
12.400	0.250	0.730	0.150	3	124.00
12.950	0.250	0.730	0.150	3	-128.00
13.500	0.250	0.730	0.150	3	-128.00
14.050	0.250	0.730	0.150	3	132.00

14.600	0.250	0.730	0.150	3	132.00
15.150	0.250	0.730	0.150	3	-132.00
15.700	0.250	0.730	0.150	3	-132.00

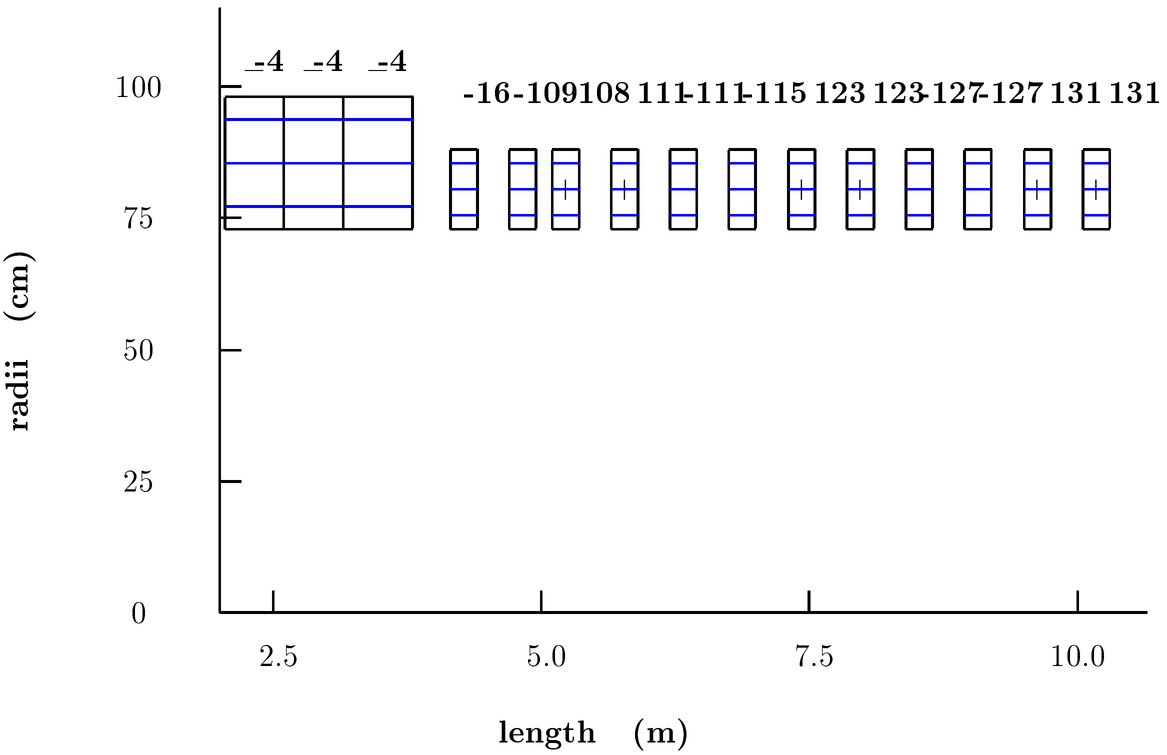

Fig. 12.

The B fields in the matching and the beta's for a range of momenta are given in the Figs.13-14 below:

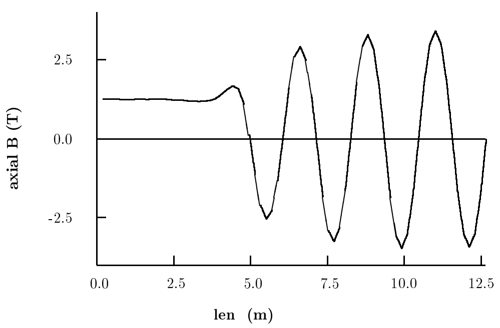

Fig. 13. Magnetic field *vs.*distance in the matching to the FOFO section

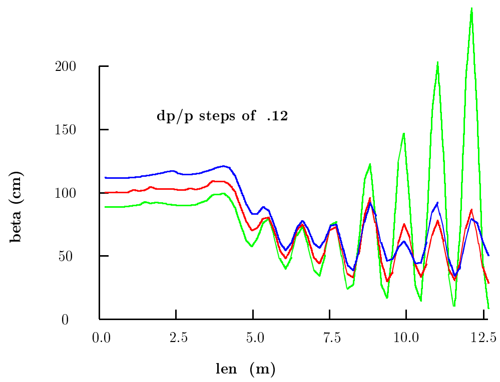

Fig. 14. Beta function in the matching to the FOFO section

G. FOFO lattice

The same lattice is used in the bunching and subsequent cooling. The dimensions and current densities of the coils of 2 cells are:

Table 9. Parameters for a FOFO lattice

length	dl	rad	dr	I/A
m	m	m	m	A/mm^2
0.250	0.600	0.730	0.250	57.60
1.350	0.600	0.730	0.250	-57.60

These coils and B fields on axis for the FOFO are shown in the following Figs.15-17:

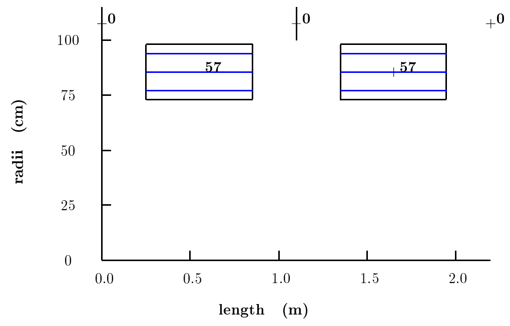

Fig. 15. Schematic of one cell of the FOFO lattice

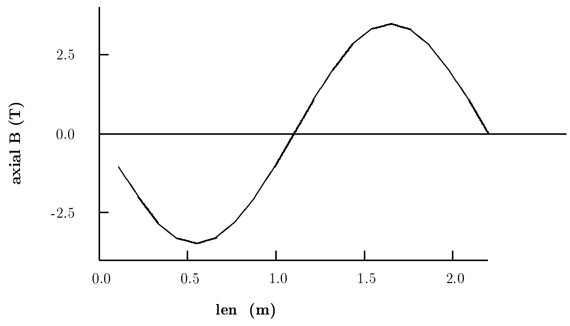

Fig. 16. Magnetic field in one cell of the FOFO lattice

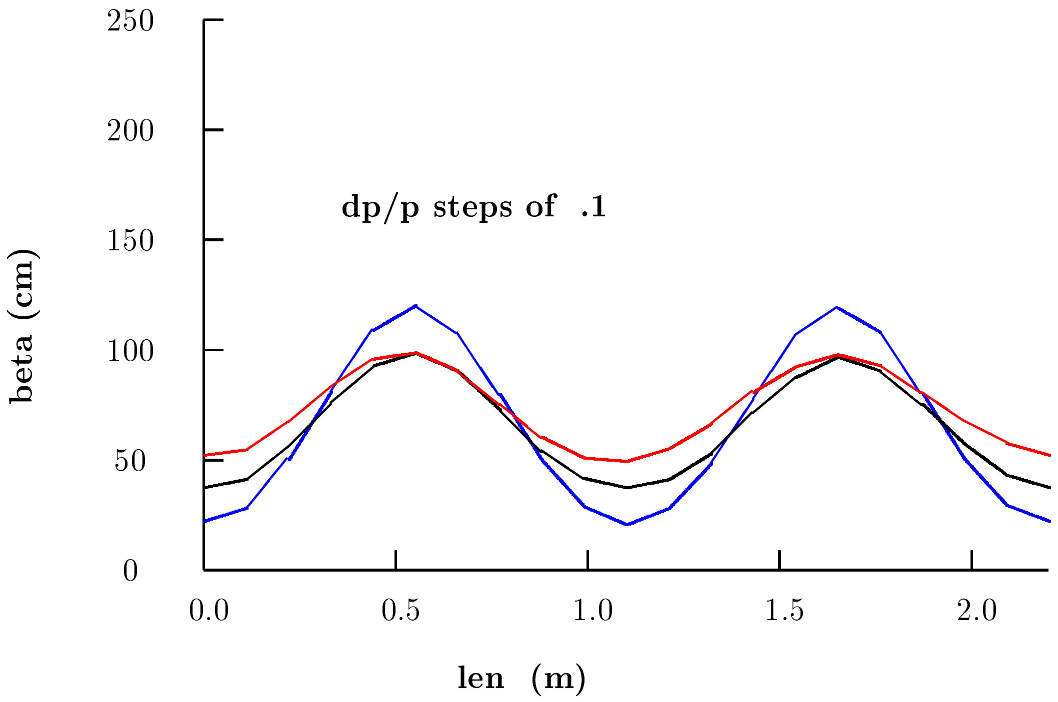

Fig. 17. Beta function in one cell of the FOFO lattice for different momenta

H. Bunching

Bunching is performed by two stages, each consisting of 175 MHz rf, second harmonic (350 MHz) rf, and a drift. The frequencies used are chosen to be a multiple of 350 MHz, the frequency of the LEP sc cavities that are assumed to be used in the later acceleration. The 175 MHz cavities are placed at the high beta locations, just as in the cooling (see below), but the 350 MHz cavities are at the beta minima, where the hydrogen absorbers are in the cooling. Two cells are used for rf in the first stage, followed by a first drift (21 m). 3 cells are used for rf in the second followed by the second drift (11 m). The arrangement is illustrated in Fig.18

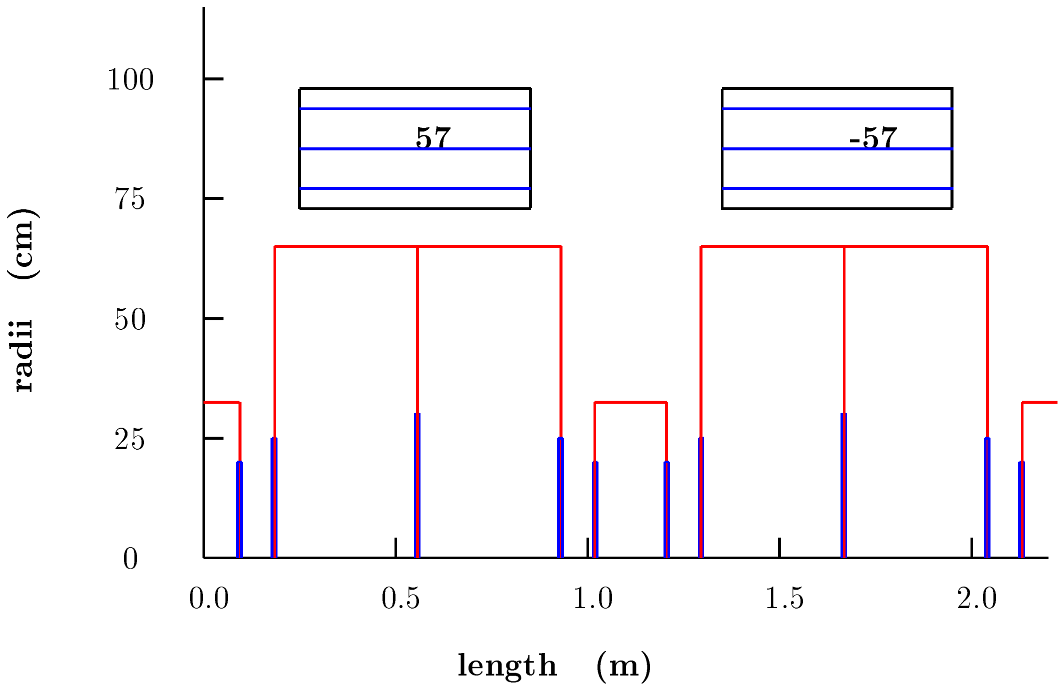

Fig. 18.

Table 10. Parameters for the bunching section

frequencies	175 and 350 MHz
gradients	8 MV/m and 6.66 Mv/m
drifts	19 and 10 m
bunches formed	52
initial rms dp/p	3.6 %
final rms dp/p	9 %

Momentum *vs.* ct (modulus one wavelength) and the rf induced changes of energy are shown in Figs.19-25

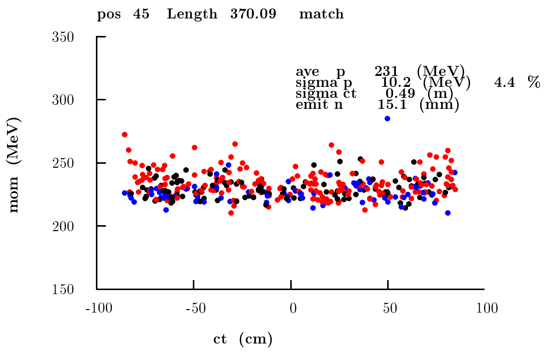

Fig. 19. Longitudinal phase space at the first drift

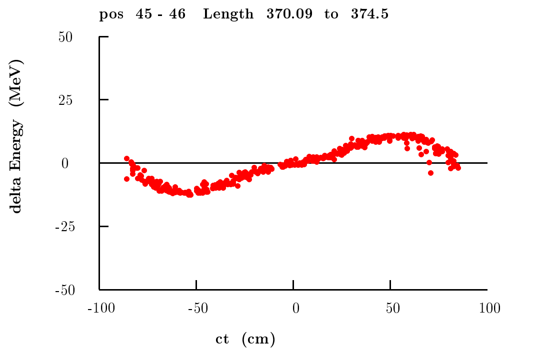

Fig. 20. Change of energy *vs.* c-time

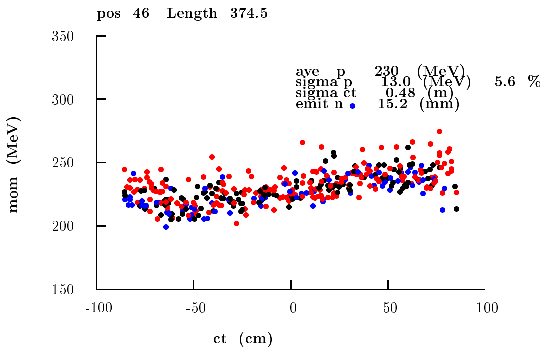

Fig. 21. Longitudinal phase space at ...

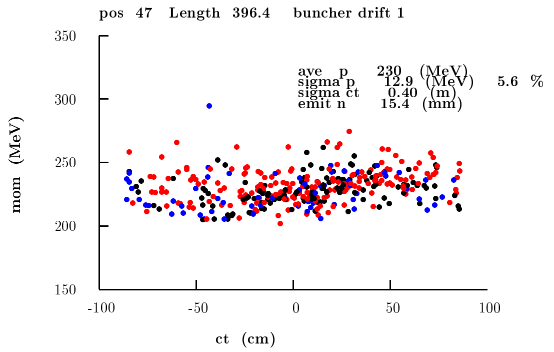

Fig. 22. Longitudinal phase space at ...

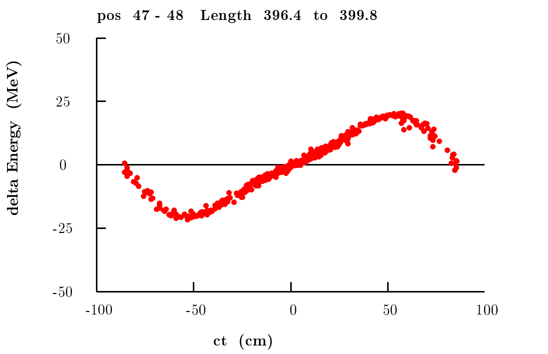

Fig. 23. Energy change *vs.* c-time

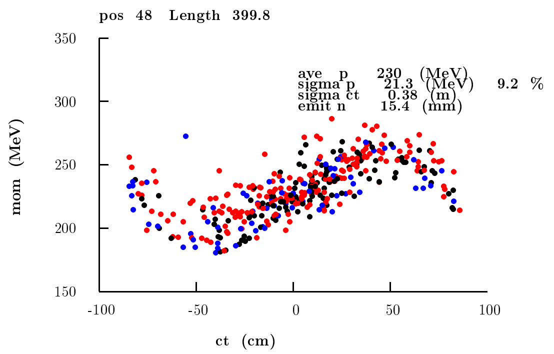

Fig. 24. Longitudinal phase space at ...

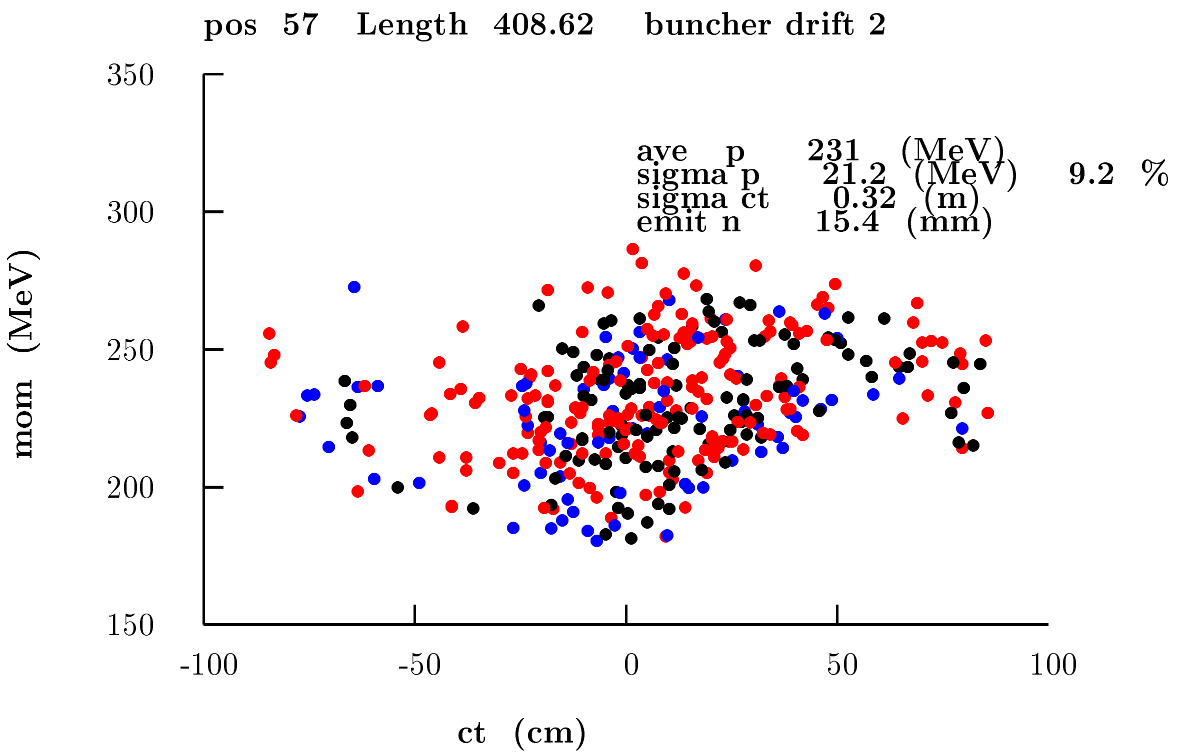

Fig. 25. Longitudinal phase space at ...

I. Cooling

A simple comparison of the total produced six dimensional emittance and the total acceptance of a plausible storage ring indicates that cooling might not be needed. But without cooling, the muon accelerator would have to have a transverse acceptance of about 100 π mm rad. This, as we have shown, is possible with large aperture solenoid focusing and low frequency rf, but would be difficult and expensive for the accelerator.

A more reasonable acceleration scheme might have a transverse acceptance of 9.35 π mm rad., and a longitudinal acceptance of 71 π mm rad. (= 0.025 eV s). The following cooling is designed to match into this acceptance.

The current simulation, using a fixed lattice, cools to below 3 π mm rad.. This is larger than the originally specified 1.5 π mm rad., but because the distributions are truncated, a high fraction of the beam is accepted into the specified 9.35 π mm rad. aperture. The coils have been specified above. The rf gradients are 14 MV/m on the z axis. The absorber, windows and rf dimensions are shown in the Tb.11

Table 11. Parameters for one cell of the cooling section

		part 28	1 m	part 46	2 m
	mat	len cm	rad cm	len cm	rad cm
Absorber	hydrogen	14	20		
window	Al	.04	20		
space		10.7			
rf window	Be	.025	25	.0125	20
rf gap		37.3	65		
rf window	Be	.05	30	.025	25
rf gap		37.3	65		
rf window	Be	.025	25	.0125	20
space		10.7			
window	Al	.04	20		

This is illustrated below:

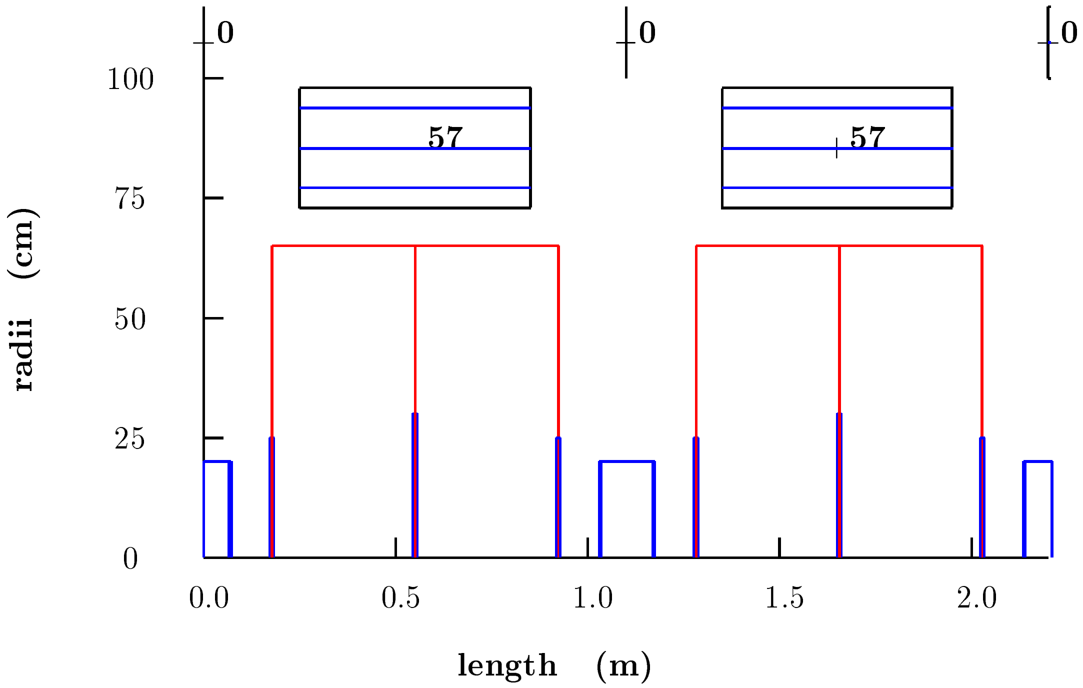

Fig. 26. Cooling cell

The transverse and longitudinal emittances *vs.* distance are:

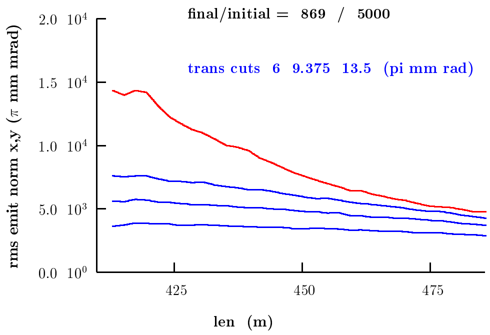

Fig. 27. Transverse emittance *vs.* distance z (m)

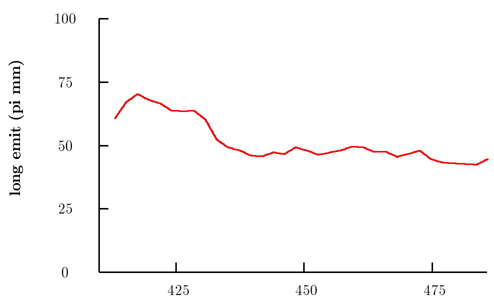

Fig. 28. Longitudinal emittance *vs.* distance z (m)

The emittances are plotted

1. with no cuts,

2. with transverse acceptance cuts at 13.5, 9.35, and 6 π mm rad.,

3. with the same transverse cuts together with a longitudinal cut at 71 π mm.

The cuts are on the amplitude parameters J, the definition of which are:

$$J_\perp \;=\; \beta_v\,\gamma_v\,\frac{\frac{x^2}{\beta} + x'^2\,\beta + \frac{y^2}{\beta} + y'^2\,\beta}{4}$$

$$J_\| \;=\; \beta_v\,\gamma_v\,\frac{\frac{z^2}{\beta_s} + \frac{dp}{p}^2\,\beta_s}{2}$$

β_s is the synchrotron $\beta_s = \sigma_z/(\sigma_p/p)$. It is assumed the α's to be zero in all dimensions. With this convention, the average of the J's are equal to the normalized emittances, as normally defined. The average of any one term would gives the emittance, hence the number in the denominator equals the number of terms. Note that the x and y amplitudes are combined to correspond to circular apertures, but the definitions are for the normally defined separate x and y emittances.

These emittances are all significantly larger than that previously estimated for the PJK[1] front end (1.5 π mm rad.). Further cooling reduces the emittance, but is found to also reduce the number of muons accepted by the accelerator. In this example, the cooling length was chosen to maximize the number of muons accepted by 6 π mm rad. transverse, and 71 π mm longitudinal. See below:

The muons per initial proton:

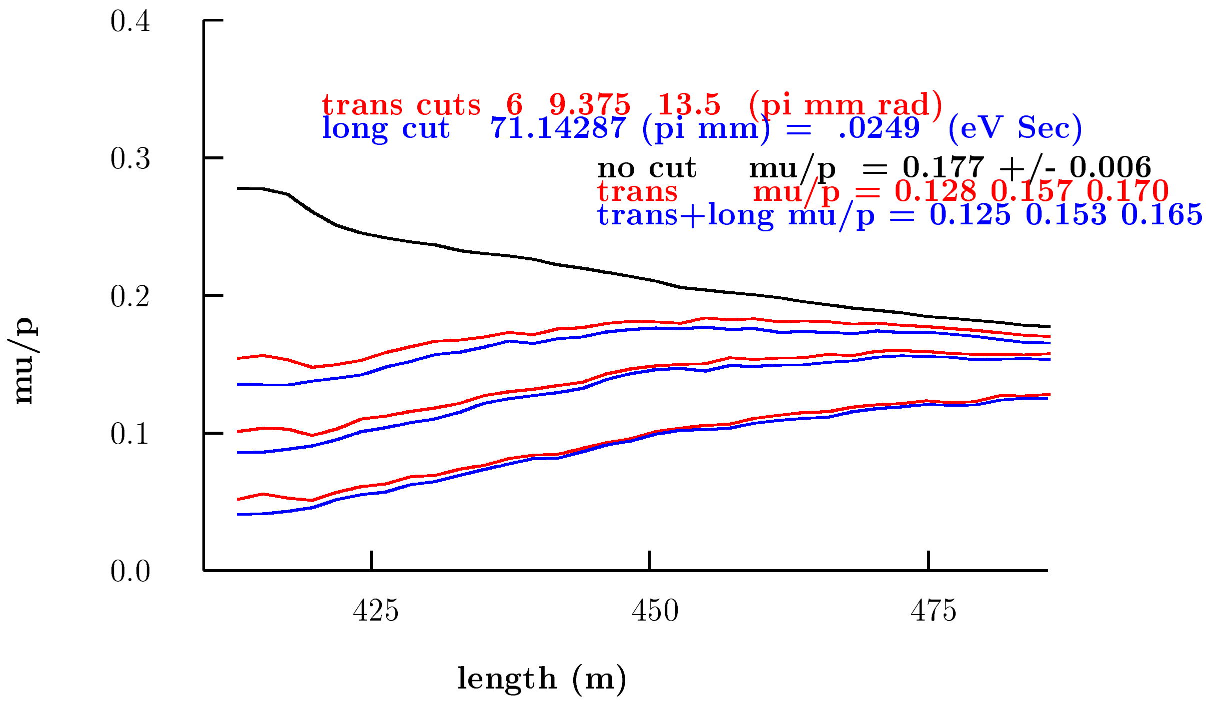

Fig. 29. Ratio $\frac{\mu}{p}$ *vs.* distance z (m)

3. Summary

A. Plots *vs.* length

The following plots show the values of some representative parameters as a function of length through the full system.

The first plot shows the axial magnetic field; it starts at 20 T and is rapidly tapered down to 1.25 T at the position of the first rf cavity of the first phase rotation. It is reversed in the middle of the mini-cool, and reversed back again in the drift that follow. After the match into the FOFO, with its ± 3.4 T fields, the fields are only plotted between cells where the fields are zero, but the same almost sinusoidal variation, though not seen, continues to the end.

The second plot shows the rms beam radius and maximum particle radii. Both are seen to be rise during the field taper, and remain near flat in the phase rotations section, but rise and fall in the two matched field reversals where the beta functions are larger. After the beam is matched into the FOFO channel, the radii are only shown between the cells, at the centers of the absorbers, where the beta function is at a minimum. Because of this smaller beta, the rms beam radius is substantially reduced. In the cooling section it is further reduced by about a factor of two as the emittance is reduced.

In the rms momentum plot, the red line indicates rms momenta with cuts applied after the first phase rotation to select the rotated particles and reject the tail of unrotated high, and very low, ones. This cut is not a physical one. The blue curve gives the larger spread of all the particles including the tails. The rms emittance is seen to drop rapidly in the first few meters as the acceptance of the channel cuts off large transverse momentum pions. It is reduced in the mini cooling, although there is clear evidence of some emittance blow up in the field reversal. The emittance then remains conserved until the cooling where it drops as expected.

something is missing here

The mu/p plot shows the loss of particles in the mini cool as the lowest energy pions are stopped in the hydrogen. The losses in the drift and induction linac are almost entirely from decays. The early step in number of muons after the start of the cooling come from the scraping of bunch tails remaining after the buncher. Later, straggling in the absorbers would cause the longitudinal emittance to grow, but since the bucket is already full, this leads to the steady loss observed.

In the average energy plot one sees a consistent difference between the average and the reference momenta. This arises because of the slower forward motion of large amplitude tracks that is matched by a zero amplitude reference at a lower energy. At the end, as the cooling reduced the amplitudes, this difference is seen to decay.

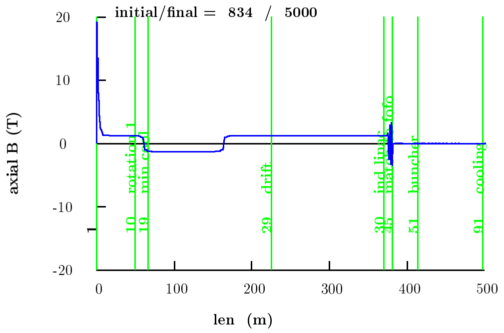

Fig. 30. Magnetic field *vs.* distance z (m)

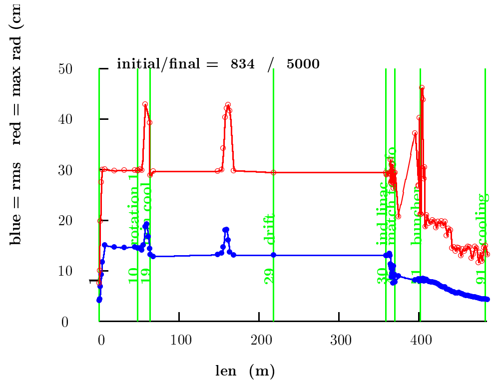

Fig. 31. *rms* Beam radius blue and maximum beam radius red *vs.* distance z (m)

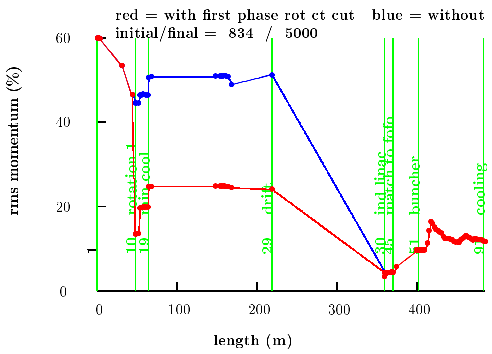

Fig. 32. *rms* momentum *vs.* distance z (m)

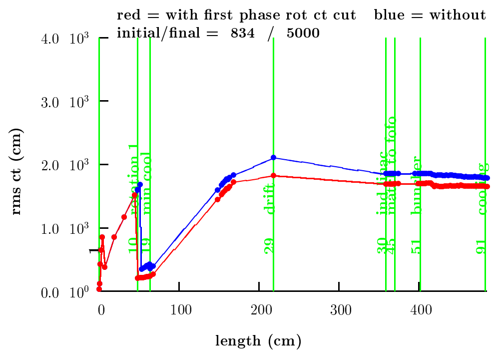

Fig. 33. *rms* c-time *vs.* distance z (m)

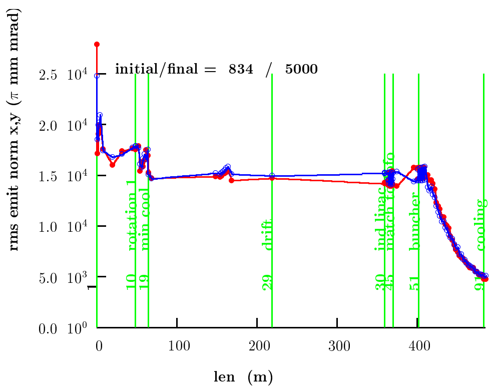

Fig. 34. *rms* normalized emittance *vs.* distance z (m)

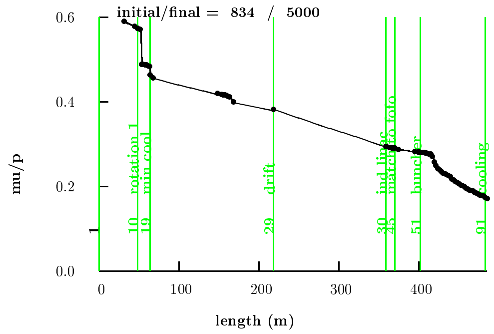

Fig. 35. $\frac{\mu}{p}$ *vs.* distance z (m)

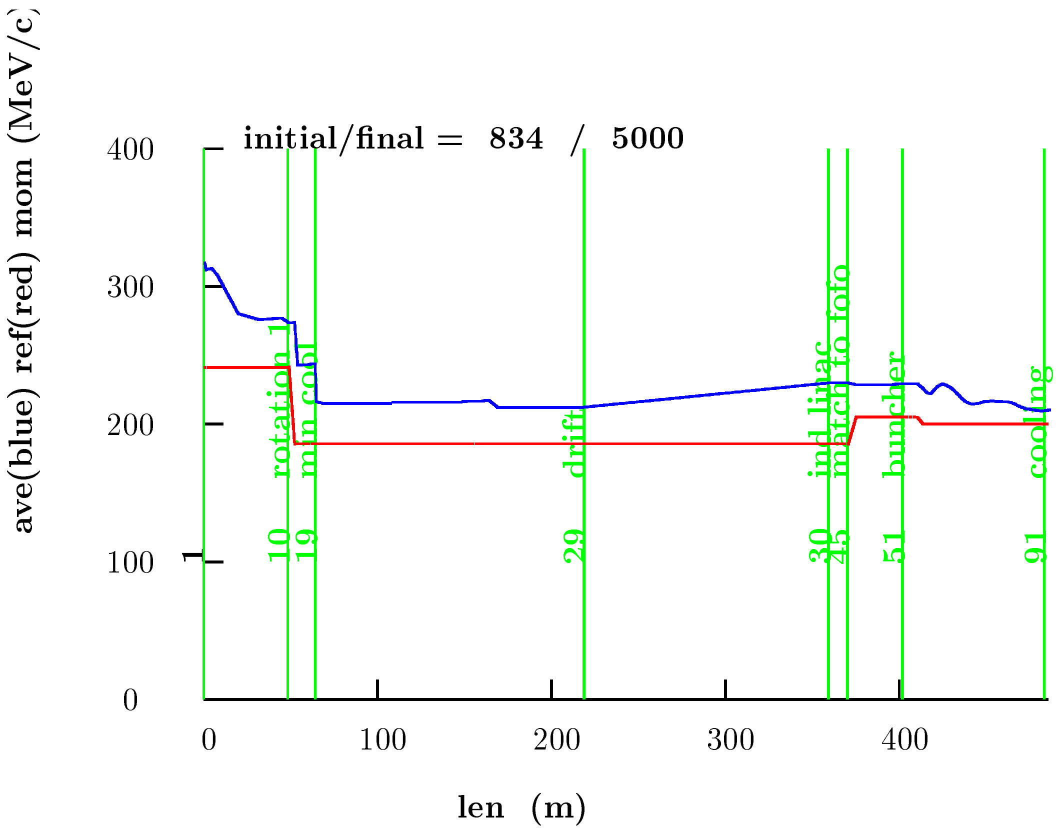

Fig. 36. Average and reference particle momentum *vs.* distance z (m)

B. Energies of pions used

In this plot we show the distribution of initial pion kinetic energies. In black, the distribution is for all initial pions, in blue the distribution is only of those initial pions that made muons present at the end of the system. The red line shows the ratio of these two, *i.e.* the efficiency of muon production as a function of the initial pion energies. It is seen to span approximately from 50 to 450 MeV, with an efficiency in this range of about 20 %, with a tail of used pions to 700 MeV.

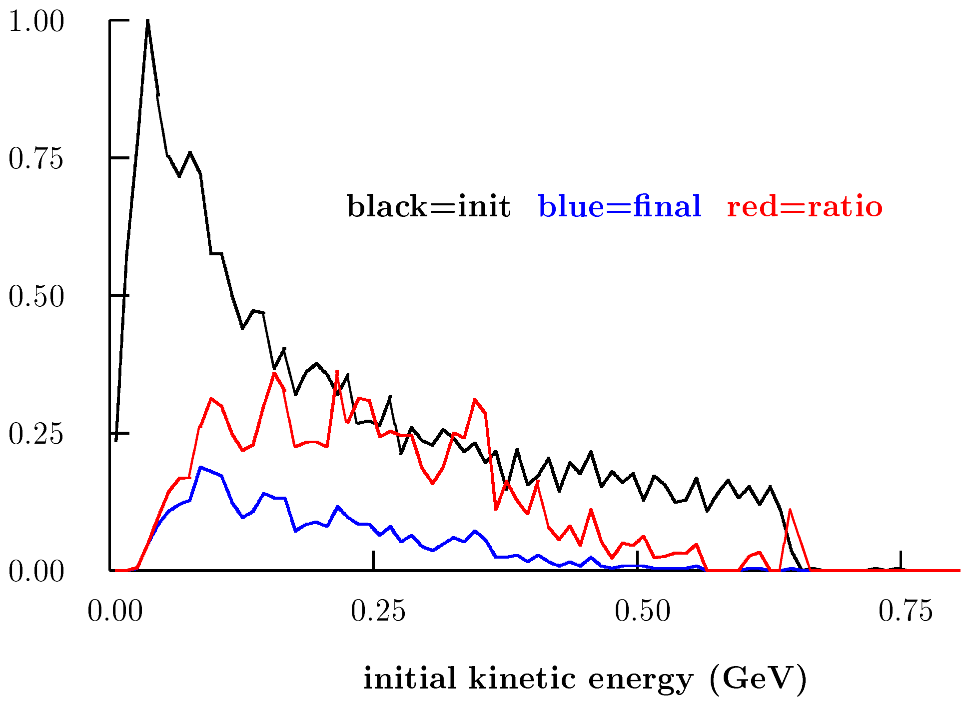

Fig. 37. Normalized energy distribution of initial muons (black), final muons (blue) and ratio $\frac{\text{final}}{\text{initial}}$

C. Comparison with other systems

Compared with estimated performance of such a system in the PJK paper[1] and Parameters Document[10], the number of muons per proton is a little higher (0.18 compared with 0.13), the longitudinal emittance is about the same ($\approx 30\ \pi$ mm), but the transverse emittance is larger (3 π mm rad. compared with 1.5 π mm rad.). Thus, this study, using ICOOL, substantially confirms the earlier, but less accurate estimate.

We have also run ICOOL on a sequence of other systems, all using the same cooling and approximately the same induction linac acceleration voltage swing. These studies were not carefully optimized and thus the comparisons with them may favor the *base* example that is the subject of this paper. However, it is noted that the performance of the last example, which shares many features with the Feasibility Study case[10], has achieved the same number of muons per proton (0.015 mu/p).

The following table Tb.12 gives the approximate factors, and their cumulative effect, as various modifications are made to the above system: The factors have statistical accuracies of ≈ 7 %, and, in the final two entries, much larger possible dependencies on the details of the examples studied. Also given, are the number of muons per proton and the numbers of muon decays per year achieved with 1 MW proton drivers. It is assumed that 40 % of the storage ring circumference is used, and that the acceleration efficiency is 80 %.

Table 12. Comparison factors to results of similar systems

Change	factor mu/MW	cumulative	μ/p	μ decays/year
80 MHz rf to 3 m from target	1.07	1.07	.16	1.3 10^{20}
Base	**1.0**	**1.0**	**.15**	**1.2** 10^{20}
increase σ_t from 1 to 3 ns	.7	.7	.105	.85 10^{20}
change p energy 24 to 16 GeV	1.0	.7	.07	.85 10^{20}
remove first phase rotation	.5	.35	.035	.42 10^{20}
change target Hg to C	.6	.21	.021	.25 10^{20}
shorten drift to 50 m	.6	.13	.015	.16 10^{20}

With the changes described below we may hope to raise the efficiencies of any of these examples by as much as a factor of two, but the ratios between them are probably going to persist.

D. Possible changes and improvements

- Mercury Target

  As noted in the target section, the mercury target simulated here would probably not survive for the required 2μs of spill at the BNL-AGS at 1 MW (10^{14}), although it might well be OK with the smaller number of protons per spill (2.5 10^{13}) in Fermilab. Two ideas have been considered:

  1. Deliberately blow up the emittance of the proton beam and focus it towards the back of the target.
  2. have four/six separate 3 mm beams side by side. *e.g.* 6 beams spaced by 1.2 cm (center to center) for a total spread of 6 cm. The proton beam is then swept across them so that only one bunch enters each target.

  Item 1) might reduce the temperature by a factor of 2-4; 2) reduces it by 6, and the resulting temperature rise would then be around 200-400 degrees, which is almost certainly acceptable. Conceivably, either item 1) or 2) might suffice alone.

- Taper down from 20 T The taper used falls to 1.25 T in about 6 m. This is theoretically too fast for the highest pion momenta captured ($\approx$ 700 MeV). It may be advantageous, therefore, to use a slower taper.

- Improved field reversal

  It was noted above that there is considerable particle loss in the field reversal between the absorbers of the mini-cooling, but little loss in the field reversal in the second phase rotation drift. This must be understood, and may require redesign of the first reversal.

- Match Amplitude momentum correlation

  Large amplitude particles, of a given momentum, have longer paths, and lower forward velocity, than low amplitude particles. In order to propagate in an rf lattice, such as the cooling channel, the large amplitude particles must have higher momentum than the lower ones: finite correlation between amplitude and momentum. Such a correlation arises naturally in the phase rotation, and could, in principle have the required value for the cooling; but such is not the case here. The correct correlation could be obtained in various ways, the simplest of which would be to raise the axial magnetic filed in the drift and linac. If this were done, transmission should be improved.

- Undistorted second phase rotation

  If phase rotation is achieved by a simple drift followed by a linac with fixed pulse shape, as was done in the second case here, then relativistic effects cause the rotated energy spread to be larger at short times (from initial high energies) and smaller at later times (from low initial energies). This effect can be clearly seen in Fig.10. As a result, the bunched rf buckets are overfilled by the early muons and under filled by the later ones. This distortion can be removed if at least two different linac pulse shapes are used. The use of such non distorting phase rotation should improve transmission after the bunching.

- Increase cooling longitudinal acceptance

  The cooling channel used here has an effective acceptance of about 70 π mm, and there are few particles with amplitude above this. Yet the accelerators designed for the Feasibility Study are claimed to accept 140 π mm. which would be excessive for this case. One could either:

  1. reduce the acceptance of the accelerators, and thus reduce their cost; or

2. use a cooling channel with larger acceptance (as was done in Balbekov's paper[11], and gain transmission of muons.

4. Conclusion

The physics study[12] concluded that to do the most interesting known physics, one needs a muon storage ring yielding 2×10^{20} muons per year decaying in a straight section facing a detector. Although, with a 1 MW proton source, the current design falls somewhat short of this (1.2×10^{20}), we conclude that the desired $2\ 10^{20}$ is probably achievable with the further improvements described above. The physics report notes that for the expected oscillations, polarization is not strictly needed. However, if there are unexpected effects, as one would wish, polarizations ability to change the ratio of μ and e neutrinos could become an essential feature in determining the nature of the new effect. But it is clear that to reach such a performance, one may need all possible features that increase efficiency. Whether such features increase the total cost is unclear, but they certainly demand significant R & D.

REFERENCES

1. R. B. Palmer, C. Johnson and E. Keil, *A Cost Effective Design for a Neutrino Factory*, BNL-66971, CERN SL/99-070 AP, Neutrino Factory Note 0.9; also as a Muon Collider Note muc0067
   http://www-mucool.fnal.gov/mcnotes/muc0067.ps

2. Contribution to the Proceedings can be found at
   http://muonstoragerings.cern.ch/Welcome.html (follow the links to Neutrino Factory and Workshop)

3.

4. J. C. Gallardo and R. B. Palmer, *MCM: Fortran program to simulate the front end and cooling section*, unpublished

5. R. Fernow, *Fortran program to simulate front end and muon ionization cooling*

6. N. Mokhov, *The MARS code User's guide*
   http://www-ap.fnal.gov/MARS/

7. H. Kirk, unpublished

8. C. Ankenbrandt, *et al.*, *Status of Muon Collider Research and Development and Future Plans*, Phys. Rev. **AB**.....

9. Y. Fukui, *Simulation of the pre-cooling stages of the neutrino factory*, Muon Collider Note muc0055
   http://www-mucool.fnal.gov/mcnotes/muc0055.ps

10. N. Holtkamp and D. Finley, *DRAFT: Feasibility Study.....*, unpublished.

11. V. Balbekov, ... , Muon Collider Note muc00xx
    http://www-mucool.fnal.gov/mcnotes/muc00xx.ps

12. S. Geer and D., *DRAFT: Physics Study.....*, unpublished.